Mechatronics Characterization of a Novel High-Performance Ergonomic Exoskeleton for Space Robotics Telepresence

A. Schiele*, H.-P. Seiberth**, P. Klär**, G. Hirzinger***

*Telerobotics, Haptics and Human-Robot Interfaces Laboratory, ESA, Netherlands
e-mail: Andre.Schiele@esa.int

**University of Applied Sciences Kaiserslautern, Zweibrücken,Germany
e-mail: patrick.klaer@fh-kl.de

***Institute for Robotics and Mechatronics, German Aerospace Centre, DRL RM, Germany
e-mail: gerd.hirzinger@dlr.de

Abstract

This paper introduces the mechatronic design of the X-Arm-2 haptic exoskeleton. The X-Arm-2 is a new and fully actuated force-reflecting human arm exoskeleton, based on our previously proposed ergonomic kinematic exoskeleton structure [1]. The X-Arm-2 is the result of an overall research effort on ergonomic haptic wearable devices [2]. This effort has led to a power-dense haptic device design that is explicitly human-centered. The X-Arm-2 can a) interact with varying operator arm sizes without requiring adjustments *(5^{th} – 95^{th} %-ile range for Astronaut crew)*, b) provide crisp force-feedback performance through a human-oriented scaling and implementation of actuators and torque sensors, c) interact with the full workspace of the human limb without limiting natural movement and without creating interface forces [3] and d) has a low overall mass *(without motor drivers)* of only 6.2 kg. The inertia of its movable structure was minimized by re-locating some of its most powerful drives via Bowden cable transmissions [4].

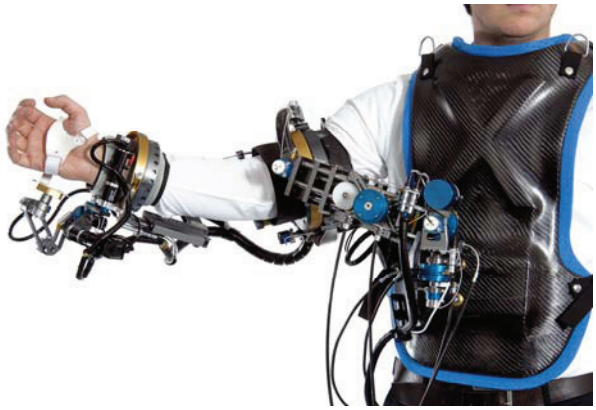

Fig. 1: Overview of the X-Arm-2 exoskeleton while being worn by an operator. The X-Arm-2 haptic device possesses 14 degrees of freedom (d.o.f.), out of which 8 are actuated by highly power-dense DC actuator units. Each joint-output is equipped with a high-resolution torque sensor. Some joints are remote-actuated by Bowden-cable transmissions. The kinematic design of the exoskeleton is highly ergonomic, to fit users ranging from the 5^{th} – 95^{th} %ile of Japanese Female to US male population (ISS crew range), without requiring mechanical adjustments. In total, the wearable, ergonomic X-Arm-2 weights only 6.2 kg.

1 Introduction

In the past years, ESA has carried out research to optimize the design of the exoskeleton for use inside the International Space Station. The X-Arm-2 shall enable telerobotic operations with force-feedback from within a weightless environment *(therefore a bodygrounded design is a must)*. In particular, during the design phase, focus was on the drive-system optimization [4], the kinematic design optimization [1], the acceptance and ergonomic-feel to users [3] as well as on the feasibility to control and map to remote robots [5]. The overall research effort on truly human-centered exoskeletons [2] has culminated in this first implementation of a full haptic exoskeleton with 8 actuated degrees of freedom. It is the goal of this paper to introduce the underlying design principles and the actual mechatronic implementation of the new X-Arm-2 haptic exoskeleton.

2 X-Arm-2 Design Rationale

2.1 Design heritage

The X-Arm-2 incorporates the same kinematic design principles proposed earlier by us in [1]. A general overview of the X-Arm-2 exoskeleton is shown in Fig. 1. The most striking kinematic difference w.r.t. previous prototypes is the reduction from sixteen to only 14 degrees of freedom *(d.o.f.)*. Moreover, following additional changes have been performed on the overall mechanical structure:

- The joint parameters were slightly modified to tolerate larger user variability without producing noticeable interface loads during movement. Such up-dates were based on experimentation and findings reported in [3].
- The spherical joint-group around the upper-arm attachment was implemented with a carbon-fibre mono-wing, which reduces mechanical protrusions

into the workspace between human arm and torso.
- The diameter of the upper-arm and fore-arm enclosures was increased to fit also users with larger arm diameters.
- The new exoskeleton is fully actuated and sensorized.

2.2 Optimization *for* the human

In order to be maximally human-centered and ergonomic in its design, to be portable and to be a good haptic device at the same time, besides it's specific kinematics structure, the exoskeleton has been optimized to meet the following overall targets:

1) Minimize the overall mass and maximize the actuator power-density.
2) Adjust the actuator and sensor performances such, that they optimally fit the 'human needs'. This means that maximum power is required most proximally *(near the shoulder)*, while maximum torque controller performance is required most distally *(near the wrist)*.
3) Maximize the dynamic range, minimize friction and backlash, implement a back-drivable and low-inertia device, to fulfill the general requirements for good haptic device design.
4) Implement the exoskeleton as an impedance-type device, which will likely result in lower overall mass.

All of the above targets were reached by adopting following design principles:

- Re-locate the most power-demanding actuator units by means of Bowden-cable transmission such, that they can be located outside the movable exoskeleton structure *(i.e. on a back-back unit)*. This reduces overall mass and inertia of the movable structure.
- Incorporate joint-torque sensors on each joint to be able to control joint-torque directly and to have less stringent requirements on device overall stiffness.
- Implement the actuator units with a combination of planetary gear-stages, and capstan reducers, to optimize for specific power, power density and to minimize backlash on the output.
- Optimize the gear reduction ratios to provide most optimal power transfer to the link *(load inertia and reflected motor inertia matching)*. This optimizes motor response and dynamic range.
- Scale the actuators according to need of the adjacent human limb joints, thus scaling power and size down from shoulder to wrist.
- Ensure that the torque control performance exceeds the 'human sensitivity'. The human torque Just Noticable Difference *(JND)* is always approx. 1% of the total torque *(Webers Law)* [6]
- For torque feedback, overall actuator torques should be equal to approx. $1/5^{th}$ of the maximum torque a human joint can exert in a controlled way.

3 Mechanical Sub-system

3.1 Kinematic structure

The X-Arm-2 incorporates 6 joints for interaction with the human shoulder-girdle. Four of the six joints are actuated, to provide feedback to shoulder ab-/adduction *(joints 1, 3)*, flex-/extension *(joints 2, 3)* and upper-arm rotation *(joint 6)*[*]. The shoulder structure is depicted in Fig. 1.

The elbow-articulation consists of three joints. Two are actuated: Joint 7 for feedback to elbow flex-/extension and joint 9 for pro-/supination.

For interaction with the wrist, the X-Arm-2 possesses five joints, out of which 2 are actuated to support torque reflection to wrist flex-/extension *(joint 10)* and ab-/adduction *(joint 11)*. The wrist structure is depicted in Fig. 4. As in [7], the exoskeleton attaches to the operators chest, it's upper-arm, forearm and to the palm.

3.2 Mechanical implementation

The overall mass of the X-Arm-2 is only 6.2 kg. This was achieved by using lightweight construction materials and extensive mechanical structure optimization. The chest-vest and all large links of the X-Arm-2 have been manufactured from carbon-fiber composite material and were dimensioned beforehand by means of finite element method *(FEM)* computations.

All joint-axles have been manufactured from Titanium, whereas all remaining structural parts have been implemented in hard-anodized aluminum *(AlEco62Sn^{TM})*. CNC techniques were heavily employed to manufacture the structurally and mass-optimized parts and to produce molds for the carbon-fiber parts. Carbon-fiber links were manufactured by hand in vacuum-bag technique.

3.3 Hand controller interface

A small hand-held control device is used as a dead-man switch and as a command interface to enable-/disable drives and to switch between various control modes of the X-Arm-2.

4 Mechatronic Sub-systems

4.1 Bowden-cable-drive actuators

The Bowden-cable principle has proven successful for haptic device usage [4]. In the X-Arm-2, three actuators for the shoulder articulation *(joints 1, 2 and 3)* and the elbow actuator *(joint 7)* have been relocated by Bowden-transmission. Each Bowden Cable Drive *(BCD)* consists of three basic elements: a) The motor-side assembly, consisting of the actuator unit, b) the transmission itself and c) the joint-side assembly.

[*] Note: Joint numbering includes also the passive non-actuated joints.

The motor-side assembly consists of a brushed DC motor *(Maxon RE-series)*, a 500 pulses-per revolution increment encoder mounted on the *(rear)*-shaft, a low reduction planetary gear reducer and a backlash-free and ultra-low friction Capstan reducer at the output. This way, the capstan reduces the planetary gear's backlash by the amount of the capstan reducers' reduction ratio! Custom made torque sensors are then located between each capstan and the input terminals of the Bowden-transmissions. An overview of the Bowden cable actuator architecture can be obtained from Fig. 2 *(right)*, which depicts the actuator transmission for the elbow articulation *(joint 7)* of X-Arm-2. On the left-hand side of Fig. 2, a close-up view on the motor-side assembly is depicted, showing the capstan *(visible, gold anodized)* and the motor-side torque sensor *(within blue anodized housing)*. On the joint-side assembly *(Fig. 2 far right)*, the transmission cables are mounted on the housing of the joint-side torque sensor *(blue-anodized as well)*, whereas the movable link is rigidly connected with the joint axle. Each joint-side output is coupled with a high-precision conductive plastic potentiometer that is used as absolute position reference.

We have shown earlier in [4] that relocation of the actuators increases the joint power-density by a factor of five and the specific power by a factor of more than six-fold, yet keeping joint performances *(torque tracking, contact stiffness, etc..)* nearly identical w.r.t not performing a Bowden-cable relocation. The BCD actuator locations within the X-Arm-2 were selected such, that despite the somewhat reduced performance, the human operator will not feel a difference. This is the case, if the torque controller resolution is higher than that of the human joint, which especially is easy to achieve for the more proximal joint locations. This means that, for the chosen locations, the BCD actuator feels like an 'ideal' haptic drive, yet, providing an extremely power-dense solution.

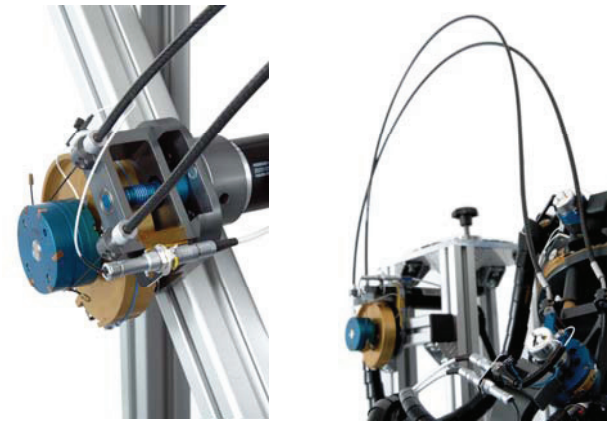

Fig. 2: Photograph showing the implementation of the Bowden-cable actuated joint on the exoskeletons elbow unit (joint 7). A magnified view on the remote BCD drive is shown on the left, whereas an overview of both, motor- and joint-side including the cable transmission is shown on the right.

4.2 High expansion-ratio rotary-to-linear actuator

In order to interact with the full workspace of the human arm, we have postulated a linear joint in [1]. Joint 3 of the X-Arm-2 is an implementation of such a linear haptic joint. The rotary-to-linear actuator has been implemented as a BCD and has an extremely high expansion- to storage-ratio of 2.4:1. Through an elegant mechanical system, this joint can be stowed with a total length of only 0.187 m, while in full expansion it can extend up to a total length of 0.455 m. Like the other BCD's in the X-Arm-2 also this linear-to-rotary actuator possesses integrated motor-side and joint-side torque sensors. The joint-side assembly of that linear actuator is shown in a close-up view in Fig. 3. From the figure, it can be already inferred that this joint is stiff against torsion.

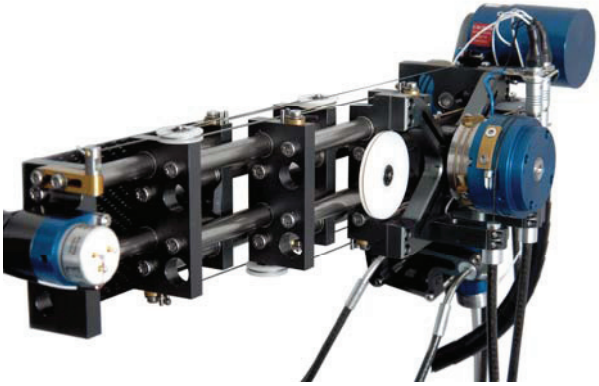

Fig. 3: Overview of the high expansion ratio linear drive that is actuating joint 3 of the X-Arm-2. The linear drive is torsion stiff, can be position or torque controlled and possess a high dynamic range. The blue cylinder shown on the front right side, contains the custom made torque sensor and the interface to the Bowden-cable transmissions.

4.3 Direct-drive actuators

The more distally located actuators on the exoskeleton require higher performance drives *(due to better human joint torque thresholds)* and less output torque. The adopted mechanical design approach for such actuator units is similar to the motor-side assemblies of the BCD's. Each direct-drive actuator *(DD)* consists of a brushed DC motor with zero cogging torque *(Maxon RE-series)*, a low planetary reduction stage, a capstan reduction stage to remove backlash and an integrated joint-side torque sensor. The close-up view on the wrist articulation depicted in Fig. 4 shows two of such drives, implemented for wrist flex-/extension *(joint 10;the visible motor-gear assembly in nearly vertical position on the figure)* and ad-/abduction *(joint 11; the assembly that extends nearly along the horizontal line on the figure)*. Fig. 5 shows a close-up photograph of the direct drive actuator of Joint 6, which feeds torque to the upper-arm rotation of the human operator. Both actuators

located on the two exoskeleton roll joints *(upper arm rotation, joint 6 & forearm pro-supination, joint 9)* follow that same principle. The basic difference of these, w.r.t. e.g. joints 10 or 11 is, that they enclose the human limb, thus, demand a different solution for measuring joint-torque.

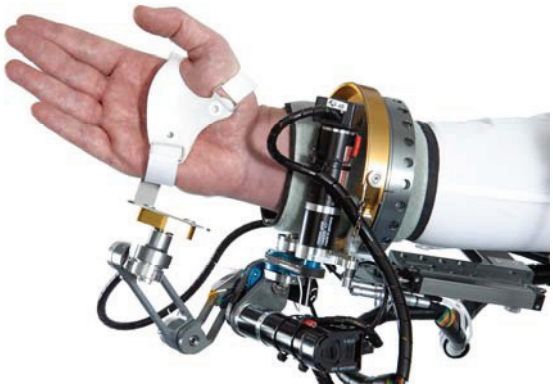

Fig. 4: Overview of the wrist articulation of the X-Arm-2 exoskeleton. Two direct-drive actuators with low gear transmission ratio actuate joints 10 and 11 of the exoskeleton. Again, torque sensors have been integrated into the output of the transmission chain.

4.4 Joint torque sensor implementations

Torque on each joint output is measured indirectly by one d.o.f. sensors using strain-gages and integrated measurement electronics. All sensors are custom-made and optimized for high resolution dynamic torque measurements. Within the X-Arm-2, there are two fundamentally different sensor types:

1) *'Direct' joint torque sensors*: On joints 1, 2, 3, 7, 10 and 11, torque can be measured rather compactly by applying strain-gages on mechanical spokes *(bending beams)* that are integrated into the motor- and joint-side pulleys of the cable transmissions or within the gear/pulley assemblies of the more distal axes. Such principle is shown in Fig. 6 *(a)*. The sensor elements depicted in Fig. 6 *(a)* are located inside the cylindrical blue-anodized housings, e.g. visible in Fig. 2 and Fig. 3. The housings have the important function to remove all normal load components of the cable transmissions themselves *(which are pre-tensioned)*. This way, the sensor behavior is highly linear and decoupled from rotation of the sensor itself.

2) *'Reaction-torque' joint sensors*: For joints 6 *(upper-arm rotation)* and 9 *(forearm pro-/supination)*, the sensor principle above is not feasible, since the human body segments protrude directly through the exoskeleton joints. The innovative approach to try measuring the reaction-torque on the actuator casing has led to a compact and feasible torque sensor solution. The drive assembly, along with the sensor element of joint 6 can be seen in Fig. 5. The implementation of joint 9 is similar *(not shown)*. Strain is measured between the input of the capstan reducer *(gold anodized visible surface in Fig.5)* and the motor casing *(black, in the background)* on two bending beams. In order to increase sensitivity, and to minimize influence of centre-of-mass *(COM)* location of the motor-assembly on the sensor element *(i.e. during motion of the entire exoskeleton and human arm)*, an additional decupling structure has been included *(visible on Fig. 5 between sensor electronics and potentiometer)*. Thus, all external load components are decoupled from the measurement, and only the pure torque transferred through the capstan reducer stage contributes to beam deformation and torque measurement. FEM models of the reaction-torque sensors are shown in Fig. 6 *(b)* for joints 6 *(left)* and 9 *(right)*.

Fig. 5: Overview of the direct-drive unit in axis 6 (for upper arm rotation). The torque sensor measures the reaction-torque on the motor casing instead of the direct output torque (since the arm passes through the middle of the joint). To remove influence of motor mass on sensor reasings, an additional mechanical decoupling structure is included. Thus, the sensitivity of the torque sensor was significantly increased.

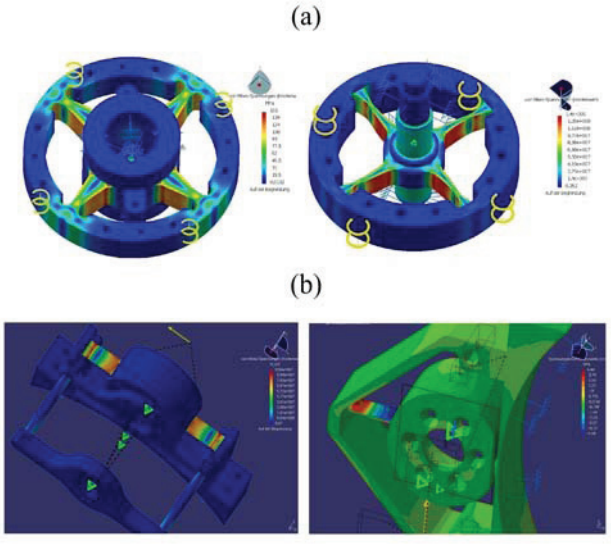

Fig. 6 FEM simulation results of some of the X-Arm-2 torque sensors. In (a, left-hand side) the sensor element of axes 1, 2 and 3 is depicted at full load of 20 Nm. On the right-hand side the pulley design of axes 10 and 11 is shown under maximum load. In (b) the reaction-torque sensor of axis 6 is depicted under full load (left), as well as the reaction-torque sensor of axis 9 (right).

For both sensor types, FEM optimization was performed on the mechanical bending-beam structures, to increase the torque sensor resolution. It was the scope of optimization to shape a peak surface strain area on each beam such that under load the peak strain is spread over the entire physical area on which the strain-gauge is applied – rather than only surfacing on a narrow strip near the corners of each beam element. This has been achieved by parametric FEM optimization. The geometry of the bending elements is not anymore box-like but curved, which can be seen well in e.g Fig. 6 *(a)*. For all sensor simulations, realistic constraints had been applied, to consider bearing constraints, tribologic contacts and correct application points and directions of loads.

Signal amplification of the small voltage across the strain-gauge full-bridges is done locally in each sensor, up to a level of 0 – 10 V. Then, the signals are fed to an external 19"-rack that contains all controller and motor amplifier hardware for the X-Arm-2. In the rack, the signals are anti-aliasing filtered, pre-conditioned by a dedicated and custom made filter-electronics board and then converted by 16-bit Analog-to-Digital converters.

5 Motion Controller Sub-system

5.1 Hardware

The controller sub-system of the X-Arm-2 is implemented in an external 19"-rack, since it was not the focus of this system to be compact and lightweight. The controller sub-system is centered on a Pentium IV PC. This PC is equipped with several PCI-cards that handle signal input from the X-Arm-2 sensors, the hand-held control device, the filter-electronics board and distribute output to the DC motor amplifiers. All control processing is implemented on the PC. Safety switches are implemented in hardware.

Current control of the motors is performed by linear amplifiers *(Aerotech BL-series, Maxon LSC-series)*, thus, extremely high bandwidth. Joint torque control loops and further high-level controllers are implemented in software, on the controller PC.

5.2 Software

In order to be maximally flexible for development and future up-grades, the entire control system of the X-Arm-2 can be easily developed and programmed from within the MATLAB™ Simulink™ and Real-time Workshop environments. Run-time executables are generated automatically from a host computer and are loaded to and executed form the target PC under the XPC Target™ operating system.

The entire control software on the X-Arm-2 PC runs at cyclic intervals in several parallel threads. Sensor acquisition, output and the entire motor torque control loops are cyclic at 5 kHz intervals. Forward- and inverse-kinematics is implemented on dedicated threads, running at 1 kHz cycle rates. Communication with external systems, e.g. slave robots to be controlled, is implemented via socket-UDP communication interfaces that can run at speeds of up to 5 kHz. Currently, however, UDP messaging is being performed at 1 kHz update rates. The network interface on the X-Arm-2 PC is a gigabit-LAN.

5.3 Joint controller structure

For now, the X-Arm-2 joint torque controllers have been fully implemented. Each joint control loop has been established with a PID controller that was tuned by making use of the Ziegler-Nichols frequency response method *(tuning on stability border)* and checked w.r.t step-response performance. On some joint axis controllers, low-pass pre-filters have been used. In order to minimize negative effects from phase rotation, Gaussian window filters have been implemented in such cases *(Gauss window low-pass implementations apply to velocity filtering mainly)*. After initialization of the X-Arm-2 via the hand-held device, bias is removed from all signals and encoder references are matched to the potentiometer absolute measurements. This way, no re-calibration is necessary after switch-on/off cycles.

For the BCD axes, which also contain motor-side torque sensors, estimates of the transmission friction are used in a feed-forward compensator. Such estimates are obtained from calculus on both, motor-side and joint-side torque sensors. This way, the effects of friction within the cable drives are nearly totally removed.

Each element in the drive-train was carefully identified with respect to its transmission characteristics, in order to be able to command precise physical quantities with the exoskeleton. Thus, the X-Arm-2 can render exact amounts of joint stiffness *(in Nm/rad)*, damping (*in Nms/rad or Nms/mm)* or general load *(in Nm or N)*, on top of simply obeying position commands. All input commands to the X-Arm-2 can be given in SI-units.

6 Performance Characteristics

6.1 Overall interaction with the human arm

Snapshots of movements within the normal human arm workspace are shown in Fig. 7. Like it's previous prototypes [1] [7], the X-Arm-2 does not obstruct natural human arm movement. It can be seen from Fig. 7 that motions in front, near and behind the operator torso are still possible. Hand-orientation can be freely chosen over the entire working-range of the exoskeleton.

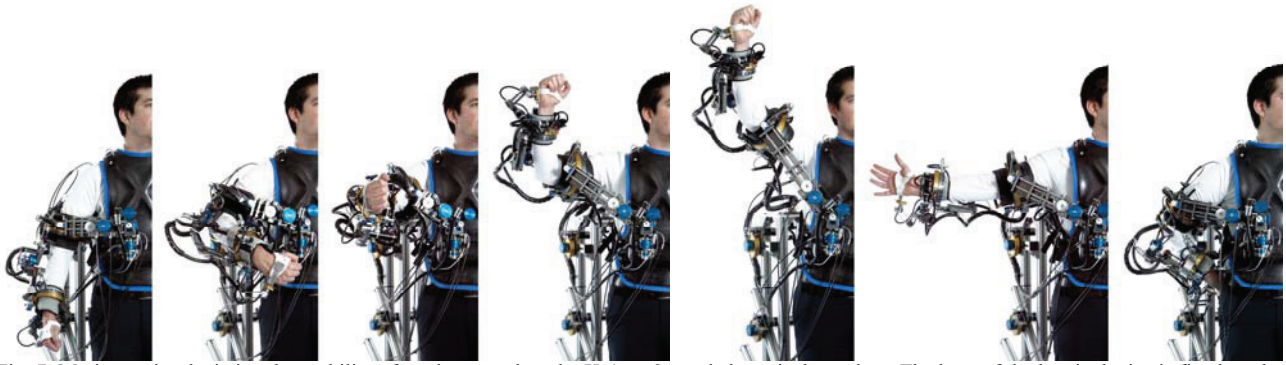

Fig. 7: Motion-series depicting the usability of workspace when the X-Arm-2 exoskeleton is dressed on. The base of the haptic device is fixed on the operator chest. Along the upper-arm and fore-arm up to the wrist, the exoskeleton comprises eight actuators for force-feedback to the human arm. This image sequence shows an excerpt of different postures that can be reached in front, besides and behind the operator torso.

TABLE I
PERFORMANCE CHARACTERISTICS OF X-ARM-2

Motor Axis No. *[#]*	Max. cont. Torque *[Nm]*	Max. peak Torque *[Nm]*	Joint output Torque Sensor Resolution *[No. of stable bit]* *	Torque Sensor linearity *[R^2]*	Gear Ratio	Backdriving Torque *[mNm]*	Measured Max. Joint-stiffness *[Nm/Rad]*
1	6.4	19.3	*8 mNm p-p = 11 bit*	*0.9998*	*35:1*	*6.6 ± 15.6*	*687.5*
2	6.4	19.3	*6 mNm p-p = 11 bit*	*0.9995*	*35:1*	*11.6 ± 27.0*	*1624.0*
3	6.4	19.3	*6 mNm p-p = 11 bit*	*0.995*	*35:1*	*7.8 ± 10.7*	*420.0*
6	2.8	8.2	*1 mNm p-p = 13 bit*	*1.0*	*33.6:1*	*0.9 ± 1.8* ***	*318.3*
7	3.0	4.5 **	*1.1 mNm p-p = 12 bit*	*0.998*	*37:1*	*16.2 ± 31.6*	*948.5*
9	0.76	1.68	*0.2 mNm p-p = 13 bit*	*1.0*	*26.6:1*	*0.2 ± 0.5* ***	*6.36*
10	0.72	2.0	*0.8 mNm p-p = 11 bit*	*0.998*	*25.2:1*	*1.6 ± 2.9*	*57.3*
11	0.72	2.0	*0.8 mNm p-p = 11 bit*	*0.999*	*25.2:1*	*1.3 ± 2.7*	*89.1*

* Stable bit resolution has been calculated based on the peak-to-peak measured noise [in mNm] when exoskeleton was powered-on fully and all drives were enabled.
** Sensor calibration artifact (nominal peak range is 8.5 Nm), thus, the resolution has been decreased artificially.
*** Friction of outer thin-section bearing not included in measurement.

6.2 General Motor Controller Performance

In Tab. 1, a summary of the X-Arm-2 joint control characteristics is provided. It can be seen that the joint axis performances are adapted to the needs, ranging from high power *(19.3 Nm output torque)* near the shoulder to low power implementation *(2.0 Nm output torque)* near the wrist. It can be seen as well, that the performance of the joint torque sensors is excellent, with a stability of 11 – 13 bit torque measurement in digital domain *(no values flipping in the 13th bit!)*. In any case, the torque sensor resolution is at all times significantly higher than the human joint torque sensing thresholds *(as indicated in [6])*. It can moreover be seen from Tab. 1 that the linearity of the torque sensors is excellent. Linearity measurements were performed under various normal-load conditions, with varying magnitudes and directions of load transfer. This shows the good functioning of the overall torque sensor assemblies, along with their enclosures and bearing supports.

In Fig. 8 the performance of joint 1 can be seen during a simulated contact with a hard wall. The input command to the joint *(red, stemming from a virtual wall contact)* is very closely tracked by the joint output torque *(in blue)*. This Bowden-cable actuated joint has a motor-side torque sensor as well (*measurement shown in green)* that is used to compute the friction feed-forward compensator terms *(in yellow)*. Since the sampling-rate of the torque controllers is high, at 5 kHz, very hard and crisp contacts can be rendered.

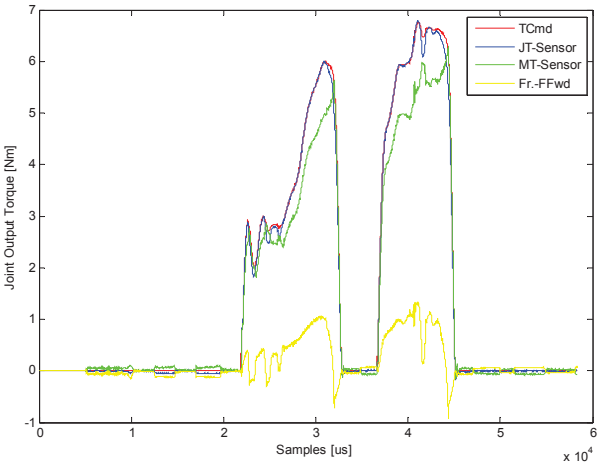

Fig. 8: Graph showing the joint-torque controller performance on axis 1 (a Bowden-cable drive BCD). The torque input command (TCmd, red) stemming from a contact with a virtual wall is closely followed by the measured joint output torque (JT, blue). The green curve depicts the measured torque at the motor-side of the joint and yellow depicts the friction feed-forward compensation terms added in the controller.

The last column of Tab. 1 gives a hint at the high maximum achievable contact stiffness that can be rendered by X-Arm-2 joints.

6.3 Actuator mechanical bandwidth

In order to quantify the mechanical performance of the drive-systems more rigorously, the mechanical bandwidth was identified for the Bowden-cable drive actuators *(BCD)* and the direct-drive actuators *(DD)* of the X-Arm-2. The bode-plot presented in Fig. 9 was obtained by measuring load transfer within two drive units from current-input to measured torque output. Input was a crested and random multi-sine current signal with a maximum of signal power centered in a frequency band ranging from 0 – 200 Hz.

To measure output torque, the output of the respective sensors had been clamped to a fixed base. It can be nicely seen from the frequency response in Fig. 9 that the mechanical bandwidth of the direct drives *(in black)* is approximately 50 Hz, whereas for the Bowden-cable drives *(in red)*, the mechanical bandwidth is still approx. 40 Hz. In both cases, this is sufficiently high for a haptic device, since the human torque control bandwidth is anyway limited to much less than 30 Hz [6].

6.4 Actuator back-drivability

The back-driving torque on the actuators is very low, which can be seen from Tab. 1. The little average back-driving torque of only about 6 mNm can hardly be felt by a human operator. For the distal exoskeleton joints, where human joint torque sensitivity is higher, the joints require only as little as 1 mNm to be back-driven.

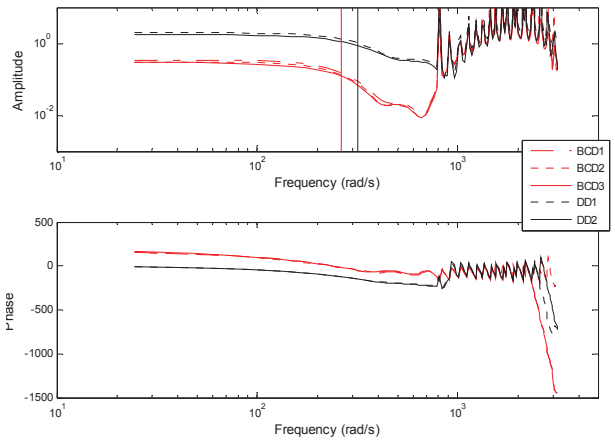

Fig. 9: Bode-plot depicting the measured mechanical bandwidth of a typical X-Arm-2 Bowden-Cable Drive (BCD) and a typical X-Arm-2 Direct Drive actuator (DD). The graph depicts several data series of Axis 1 BCD and Axis 1 in DD-mode (with the cable transmission removed). In DD configuration, the joint has a mechanical bandwidth of approx. 50 Hz (320 Rad/s, black). The mechanical bandwidth with the BCD drives is at approx. 40 Hz (255 Rad/s, red). Beyond approx. 700 rad/s the measurement is outside the region of interest and not of usage (an artifact from discrete and limited bandwidth input used for identification).

Therefore, the X-Arm-2 causes no perception of resistance during free movement. Combined with a peak maximum contact stiffness rendering of approx. 1.6 kNm/rad, this provides an extremely high dynamic range and allows to render utterly crisp and realistic contacts. The device feels 'ideal' from a human point of view.

6.5 Rendering of pure viscous damping

As a further example of the X-Arm-2 performance, Fig. 10 shows the results from a command to the linear joint 3 to emulate a pure viscous damper with a damping constant of 0.01 *(Nm s/mm)*. In this experiment, the linear joint performance was convincing, which can be seen in the recorded torque to velocity graph *(Fig. 10)*. The joint gave a sensation of high viscous damping, such as moving inside a thick, honey-like medium.

Emulation of pure viscous damping poses high demands on low drive inertia, low drive friction, stable torque measurement and good velocity filtering. Like in all other experiments, the joint controllers operated at a 5 kHz frequency.

6.6 Torque-tracking in virtual wall contacts

Torque tracking of all the X-Arm-2 joints in a simulated virtual wall environment has been recorded in Fig. 11. The high rising torque signal edges upon impact indicate the quick transition from free- to contact motion and give a visual cue of the force-feedback performance. It can be seen that towards the more distal joints *(towards axis 11)*, the rising edges become steeper, which indicates better performance of those axes.

Especially joints 6, 9, 10 and 11 show a clear 'bouncing' characteristic *(some critically damped overshoot)* upon impact, which shows the realistic behavior of rendering fast, rigid and crisp contacts.

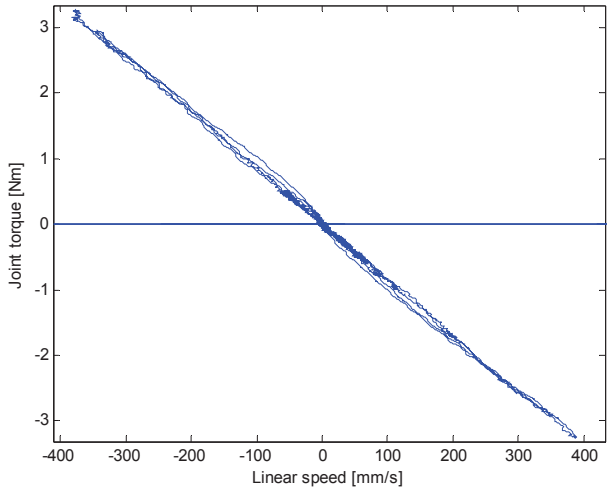

Fig. 10: Emulation of pure viscous damping, as rendered by the high-performance linear drive. The measurement shows a viscous damping behavior of the joint, when 0.01 Nm s/mm were commanded to the joint input.

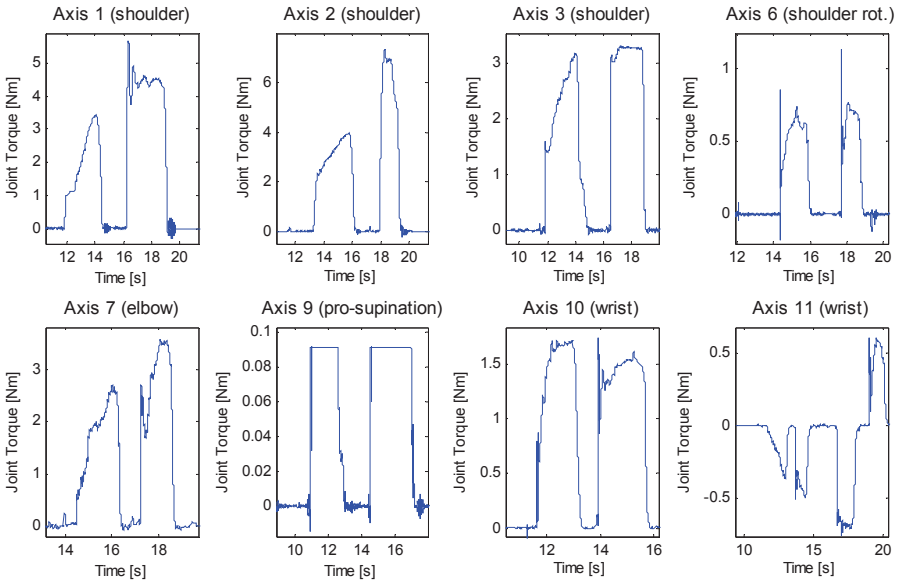

Fig. 11: Time-series depicting the torque control performance of X-Arm-2 at joint-level, during multiple impacts with varying speeds. The performance is shown for each actuated axis of the exoskeleton. High rising edges at impact show graphically the crispness of contacts.

7 Future Work

In the coming months, we will further extend the X-Arm-2 controller implementation. We plan to include gravity compensation and a refined Cartesian position and impedance control.

In terms of overall system integration, we will re-design the motor-side Bowden Cable actuator units *(that are now located on an external support-stand)* into a new compact back-pack system, which will be wearable for the operator. In context with this, all the motor controller hardware will be miniaturized and integrated with the back-pack unit as well.

Finally, we are seeking collaboration with industrial designers to develop a suitable housing, to make the X-Arm-2 exterior more rugged and appealing.

8 Conclusion

(1) An optimal synthesis between compactness of design and performance in haptic control can be reached for ergonomic exoskeletons by implementing Bowden Cable actuators in proximal and Direct Drive actuators with distal joint axes. This ensures high power-density and low overall mass while aligning power demands and sensor performance with the needs of the human joint counterparts. (2) By adopting this human-centered design, still a highly dynamic and crisp force-reflection performance can be ensured that feels 'ideal' from a human-point-of-view.

This is due to the fact that the mechanical actuator and control bandwidth is always kept higher than the human joint torque control bandwidth, and that the exoskeleton's joint sensor resolutions are significantly superior to the human joint torque thresholds at the relevant locations within the X-Arm-2.

References

[1] A. Schiele and F. v. d. Helm, "Kinematic Design to Improve Ergonomics in Human Machine Interaction," IEEE Transactions on Neural Systems and Rehabilitation Engineering, vol. 14(2), pp. 456-469, 2006.

[2] A. Schiele, "Fundamentals of Ergonomic Exoskeleton Robots." vol. Ph.D. Thesis Delft: Delft University of Technology, 2008, available at: www.library.tudelft.nl

[3] A. Schiele, F.C.T. van der Helm, "Influence of Attachment Pressure and Kinematic Configuration on pHRI with Wearable Robots", Journal of Applied Bionics and Biomechanics, Vol. 6(2), pp. 157 – 173, 2009

[4] Schiele A., "Performance Difference of Bowden Cable Relocated and Non-Relocated Master Actuators in Virtual Environment Applications", IEEE/RSJ Int. Conf. on Intellig. Robots and Syst., IROS, Nice, pp. 3507 – 3512, 2008

[5] A. Schiele, M. D. Bartolomei, and F. v. d. Helm, "Towards Intuitive Control of Space Robots: A Ground Development Facility with Exoskeleton," in IEEE/RSJ International Conference on Intelligent Robots and Systems (IROS), Beijing, 2006, pp. 1396-1401.

[6] H.Z. Tan, M.A. Srinivasan, B. Eberman, B. Cheng, "Human Factors for the Design of Force-Reflecting Haptic Interfaces", in ASME Journ. Of Dynamic Systems and Control, Vol.55-1, 1994, pp. 353 – 359

[7] A. Schiele, "Case Study: The ergonomic EXARM Exoskeleton", in *Wearable Robots: Biomechatronic Exoskeletons*, J.L. Pons Ed., John Wiley & Sons, pp. 248-255, 2008